Effect of flow channel shapes of proton exchange membrane fuel Cell on its performances

Yang Liu, Pengwei Liu, Jiyun Ren, Zunlong Jin[*], Xu Han

School of Mechanical and Power Engineering, Zhengzhou University, Zhengzhou, China
[*]E-mail: zljin@zzu.edu.cn

The shape of the cross-sectional area of the flow channel has a significant impact on the performance of the proton exchange membrane fuel cell (PEMFC). Based on the hydrodynamic calculation method, a three-dimensional PEMFC single-cell model was established. The performance of the PEMFC single cell is tuned by numerical simulations of models with different flow path cross-section shapes, and the properties of single cell such as polarization curves, oxygen distribution at different interfaces, water distribution on the cathode side, current density distribution on the cathode membrane surface and temperature distribution at the cell center section were discussed and analyzed. The results show that the dovetail flow channel has a best convection effect and the best water removal effect. At the same time, the oxygen distribution in the dovetail flow channel is more uniform, and the current density is the highest and the distribution uniformity is higher.

1. INTRODUCTION

In the past decades, with the growing global energy and environmental crisis, mankind has been exploring new energy technologies for a green and sustainable energy development future. PEMFC is attracting a lot of attention from researchers by providing near-zero emission energy conversion with high energy efficiency [1]. Besides, PEMFC has the advantages of low operating temperature, no noise, building block structure, and fast start-up, which is the most promising power generation system for future automobiles, stationary power supplies, and portable electronic devices [2, 3]. Therefore, it is a promising energy technology of the future. However, PEMFC still has many shortcomings nowadays, which prevent it from large-scale commercial application. The main manifestations are expensive market price, unsatisfactory life and stability at high temperature, insufficient technology popularity,

complicated hydrothermal management system, no perfect fuel supply system, sensitive to CO, and high catalyst cost [4]. For these reasons, numerical simulation plays a crucial role in the development of PEMFC, which is performed to further optimize its performance and cost for wide commercial application.

Among the components of a PEMFC, the bipolar plate (BP), serving as the connection between individual cells, is the key component, which accounts for more than 60% of the mass and more than 30% of the cost [5]. BP constitutes the cell channel to supply reactants (H_2 and O_2), discharge produced water, collect current and support the membrane electrolyte assembly (MEA). Therefore, the BP material should have good chemical stability and mechanical strength. Besides, the surface of BP should also be as smooth as possible (it is generally believed that the surface roughness should be less than 50 μm). From the perspective of building an environmentally friendly society, BP should preferably not pollute the environment with recyclability [6, 7]. As the uniform distribution of the reactants contributes to the uniform distribution of the reaction rate, the design of the BP flow field (size, shape, assembly method and flow direction) is a major factor affecting the performance of PEMFC [8].

There are many ways to modify the PEMFC structure to improve the cell performance, and mainly are two categories in terms of overall geometry and feature length. The first is the design of the macro structure, which determines the overall structure of the cell. The second is the design of the microstructure in the cell, which is related to the material properties of the porous electrode as well as the microstructure, such as the volume fraction of a material in the composite electrode, the porosity of the electrode, and the particle size [9-11]. So far, exploring an efficient flow channel structure is thought to be the best way to improve the performance of PEMFC, and numerical simulations have been widely used to optimize the flow field in BP [12-17]. A relatively complete review was conducted by Manso [18] in studying the effect of geometric parameters of the flow field on PEMFC. In their study, it was found that many drawbacks of the PEMFC can be overcome by proper flow field design. Problems such as water management and inhomogeneous distribution of reactants can be solved by effective design of the BP flow field to improve the performance of PEMFC. When considering the geometric parameters for optimizing PEMFC, the following points can be considered: flow field, flow direction, channel length and number of channels, use of baffles in the flow direction, cross-sectional shape, channel and rib width, channel depth, and aspect ratio of the cross-section. In previous designs regarding PEMFC flow channel shapes, Wan[19]improved the performance of PEMFC to a certain extent by designing a new M-shaped channel to optimize and improve the performance of the cell, such as heat and mass transfer, but this simulation was only for the numerical analysis of the individual components of the channel, which was too limited and did not analyze the mechanism of the cell performance improvement and the overall analysis of the cell. Some authors [20-22] performed an optimization analysis of the cell flow channel shape with the upper and lower flow channel widths as control variables and the maximization of current density as a single objective function. Their results only showed the characteristics of the current density after optimizing the flow channel shape and did not analyze the mass and heat transfer of the cell. Freire [23] and Li et [24] analyzed the effect of different flow channel shapes on the mass and heat transfer in serpentine channel PEMFC. The serpentine channel has large bends and turns, and its conclusions are not necessarily applicable to parallel direct flow channels. Therefore, the influence of flow channel shape on the PEMFC of direct flow channel still needs further discussion and analysis.

From previous studies, it can be found that most of the current studies mainly focus on the design of flow field arrangement. The development of numerical simulation has facilitated a variety of novel ideas for researchers. In this paper, computational simulations for the most widely used cell model with parallel flow fields are conducts, and also the effects of different flow channel shapes on cell performance is analyzed. This paper first introduces the computational model, including geometric configuration, control equations and boundary conditions. The model is validated for reliability. Then, the distributions of oxygen, generated water, current density and temperature at each interface inside the cell were analyzed, and the effect of flow channel cross-sectional shape on PEMFC performance was derived by comparative analysis.

2 MATHEMATICAL MODEL

2.1 Geometric model

In this study, PEMFC with different flow channel shapes were developed in the commercial software COMSOL Multiphysics based on the finite element method. The single-channel model was based on repeating cells in a sufficiently large cell stack.
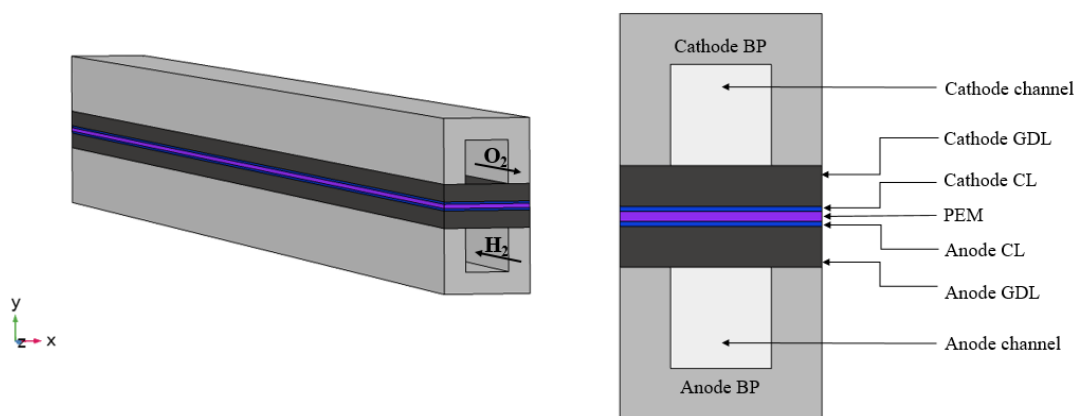

Figure 1. Schematic diagram of PEMFC structure

Figure 1 illustrates the detailed components of the PEMFC model: bipolar plate (BP), cathode/anode gas channel(CH), cathode/anode gas diffusion layer (GDL), cathode/anode catalytic layer (CL), and proton exchange membrane(PEM). Flow channel shapes have a large influence on the gas transport and thus on the cell performance. In this study, the effects of four different flow channel cross-section shapes on the overall cell performance, gas transport, current density, and temperature were analyzed. Figure 2 shows the cross-sectional shape of a single cell with four different runner shapes, namely rectangular (standard case Model 1), elliptical (Model 2), trapezoidal (Model 3), and dovetail (Model 4). The detailed geometrical parameters as well as the flow channel structure parameters are listed in Tables 1 and 2, respectively.

Table 1. Geometric details and material properties in PEMFC [25-27].

| Parameters	Unit	Value
Channel length	*mm*	50.0
Rib width	*mm*	1.0
Anode GDL thickness	*mm*	0.4
Cathode GDL thickness	*mm*	0.4
CL thickness	*mm*	0.05
PEM thickness	*mm*	0.1
GDL permeability	m^2	$1.18e^{-11}$
CL permeability	m^2	$2.36e^{-12}$
GDL porosity	-	0.4
CL porosity	-	0.3
Volume fraction of electrolyte phase	-	0.3
Density of PEM	$Kg\ m^{-3}$	1000
Specific heat of electrode	$J\ kg^{-1}\ K^{-1}$	573
Specific heat of PEM	$J\ kg^{-1}\ K^{-1}$	4000
Thermal conductivity of BP	$W\ m^{-1}\ K^{-1}$	44.5
Thermal conductivity of electrode	$W\ m^{-1}\ K^{-1}$	25
Thermal conductivity of GDL	$W\ m^{-1}\ K^{-1}$	1.7
Thermal conductivity of PEM	$W\ m^{-1}\ K^{-1}$	2

(a) Model 1   (b) Model 2   (c) Model 3   (d) Model 4
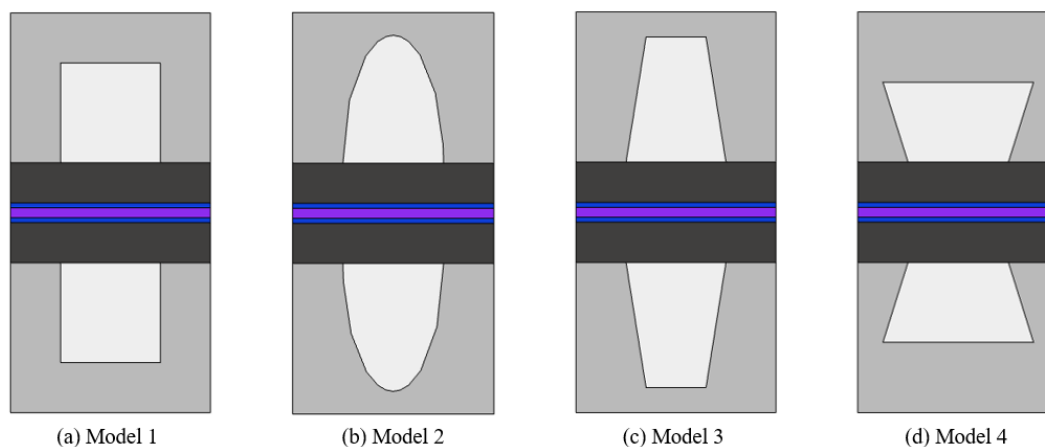
Figure 2. Schematic diagram of different shapes of flow channel structure, Model 1: rectangular flow channel; Model 2: elliptical flow channel; Model 3: trapezoidal flow channel; Model 4: dovetail flow channel.

Table 2. Flow channel structural parameters

Cross-section shape of flow channel	Width of flow channel /mm	Height of flow channel /mm	Cross-sectional area of flow channel /mm²	Flow channel contact area with GDL/mm²
Rectangle	1.0	1.0	1.0	50.0
Ellipse	1.0	1.57	1.0	50.0
Trapezoid	1.0	1.25	1.0	50.0
Dovetail type	1.0	0.8	1.0	50.0

2.2 Control equations

The numerical simulation of PEMFC involves coupled phenomena of gas flow, momentum and mass transfer, heat transfer, and electrochemical reactions. To simplify the calculation of the model, some reasonable assumptions below are applied to the 3D model.

- The model is run under steady-state conditions.
- The fluid is in laminar flow state in the flow channel.
- PEM is permeable only by protons, but not by reaction gases.
- Membrane electrode assembly are isotropic porous media.
- Reactive active sites are uniformly distributed in the functional layer of each electrode.
- Ignore the contact resistance between any two components.
- No slippage between model wall boundaries.

1)   Momentum and mass transport

The reaction gas flows through the gas flow channel and porous electrode to reach the reaction area, and the exhaust gas produced by the reaction is discharged through the outlet. The density and velocity of the fluid are continuous throughout the process, and the continuity equation can be expressed as[28]:

$$\nabla \cdot (\varepsilon \rho \vec{u}) = S_m \tag{1}$$

where $\vec{u}$ is the velocity vector, ρ is the density of the participating gas mixtures, and ε is the porosity of the porous medium ($\varepsilon = 1$ in the gas channel and $\varepsilon < 1$ in the diffusion and catalytic layers). S_m is the quality source term.

$$\rho = \frac{p}{RT}(\sum_i x_i M_i) \tag{2}$$

where p and T denote the operating pressure and temperature, R denotes the gas constant, x_i and M_i denote the molar fraction and molar mass of gas phase component i, respectively.

For the gas channel and GDL, there is no electrochemical involvement and $S_m = 0$. In the CL of the anode/cathode, due to the electrochemical reaction that takes place, the mass source term can be expressed as[29]:

$$S_m = S_{H_2} = -\frac{M_{H_2}}{2F}i_a \tag{3}$$

$$S_m = S_{H_2O} + S_{O_2} = \frac{M_{H_2O}}{2F}i_c - \frac{M_{O_2}}{4F}i_c \tag{4}$$

where M_{H_2}, M_{O_2} and M_{H_2O} are the molar masses of hydrogen, oxygen and water, respectively. F is the Faraday constant. $i_{a/c}$ denote the volume exchange current density due to electrochemical reactions at the anode and cathode, respectively.

The computational domain of the model includes gas flow channels and porous media. To solve this problem, the model uses the Brinkman equation[26]:

$$(\frac{\mu}{\kappa} + \rho \cdot \nabla \cdot \vec{u}) \cdot \vec{u} - \nabla \left\{ -P + \frac{1}{\varepsilon} \left[\psi - (\frac{-2}{3} \cdot \mu)(\nabla \cdot \vec{u}) \right] \right\} = f \tag{5}$$

where f is the volume force vector, κ is the permeability of the porous medium, ψ is the viscous stress tensor and μ represents the dynamic viscosity of the gas. The dynamic viscosity of the multi-component gas mixture of anode and cathode can be calculated as follows[30]:

$$\mu_{a,c} = \sum_{i=1}^{n} \frac{x_i \mu_i}{\sum_{j=1}^{n} \left(x_j \sqrt{\frac{M_j}{M_i}} \right)} \tag{6}$$

where μ_i denotes the dynamic viscosity of the gas phase component i .

The momentum equations for the fuel and air channels can be simplified due to the absence of the permeability term representing the porous electrodes as:

$$\rho \cdot (\nabla \cdot \vec{u}) \cdot \vec{u} - \nabla \left\{ -P + \mu \cdot \left[\psi - \frac{2}{3} (\nabla \cdot \vec{u}) \right] \right\} = f \tag{7}$$

The mass balance in the cell is described by the mass flux through diffusion and convection, and the steady-state component transport equation can be expressed as[25]:

$$\nabla \left[-P \cdot w_i \sum_{j=1}^{N} D_{ij} \cdot \nabla x_j + (x_j - w_j) \frac{\nabla P}{P} \cdot \vec{u} \right] + \rho \cdot \vec{u} \cdot \nabla w_i = S_m \tag{8}$$

where D_{ij} denotes the binary diffusion coefficient, The diffusion coefficients between the components are detailed in Table 3.

Considering the zigzag structure of the porous electrode, the binary diffusion coefficient of the porous electrode is corrected using the Brugemann correction equation[29]：

$$D_{ij}^{eff} = D_{ij} \times \varepsilon^{1.5} \tag{9}$$

2)   Heat transport

Thermal convection and heat conduction are considered in the calculation domain. The heat source of the model is mainly derived from the electrochemical heat in the catalytic layer, as well as the heat due to polarization losses. In the computational domain, it is assumed that the temperatures of the solid and gas phases in the porous electrode are locally the same. The equation for energy conservation in the steady state can be expressed as[31]:

$$\rho \cdot C_p \cdot \vec{u} \cdot \nabla T = \nabla \cdot (k_{eff} \cdot \nabla T) + Q \tag{10}$$

where C_p denotes the specific heat of the gas mixture and k_{eff} denotes the effective thermal conductivity of the porous electrode. Q indicates the heat source due to electrochemical reactions.

$$C_p = \sum_i x_i C_{p,i} \tag{11}$$

$$k_{eff} = \varepsilon \cdot k_g + (1 - \varepsilon) \cdot k_s \tag{12}$$

$$Q = |i| \cdot \left(\frac{T \cdot |\Delta S_r|}{n_e \cdot F} + |\eta_{act}| \right) + \sum \frac{i^2}{\sigma} \tag{13}$$

where k_g is the thermal conductivity of the gas and k_s is the thermal conductivity of the solid phase material. i denotes the current density, ΔS_r denotes the entropy change of the electrochemical reaction and σ denotes the ion/electron conductivity.

3)   Charge transport and electrochemical reactions

In PEMFC, the cell is fed with hydrogen as the fuel to anode and oxygen as the oxidizer to cathode. Hydrogen gas is dissociated into hydrogen ions and negatively charged electrons by the action of anode catalyst. The hydrogen ions pass through the exchange membrane and then enter the cathode side, while the electrons flow from the anode to the cathode through an external circuit connected by BP. Oxygen reacts with the electrons generated by the excitation of the catalyst to produce oxygen ions,

which then react with hydrogen ions to produce water. The flow of electrons from the anode to the cathode through the circuit generates electricity, and the chemical reaction is as follows：

$$Anode: H_2 \rightarrow 2H^+ + 2e^- \tag{14}$$

$$Cathode: \frac{1}{2}O_2 + 2H^+ + 2e^- \rightarrow H_2O \tag{15}$$
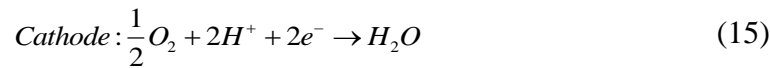
From the electrochemical reactions described above, it is clear that in PEMFC, the current can be divided into two parts: ion current and electron current. Protons pass through the PEM and form ion currents, while electrons are transferred only through the BP, resulting in currents. The continuity equation for the current is obtained using Ohm's law[32]：

$$\nabla \cdot (-\sigma_s \nabla \cdot \phi_s) = S_s \tag{16}$$

$$\nabla \cdot (-\sigma_m \nabla \cdot \phi_m) = S_m \tag{17}$$

where σ_s and σ_m are the conductivity of the electrode and membrane, respectively. ϕ_s and ϕ_m are the electron potential and ion potential, respectively. And S is the current source term. The source term in the electron and proton transport equations is the result of an electrochemical reaction that occurs only in the CLs of the anode and cathode[25]:

$$CL_{anode}: S_m = i_a, S_s = -i_a \tag{18}$$

$$CL_{cathode}: S_m = i_c, S_s = -i_c \tag{19}$$

In the charge conservation equation, the current source term is closely related to the exchange current density, which is calculated using the Butler-Volmer equation as follows[26]：

$$i_a = A_v i_{0,a} \left(\frac{C_{H_2}}{C_{H_2}^{ref}} \right)^{0.5} \left[\exp\left(\frac{\alpha_a F \eta_a}{RT} \right) - \exp\left(-\frac{\alpha_c F \eta_a}{TR} \right) \right] \tag{20}$$

$$i_c = A_v i_{0,c} \left(\frac{C_{O_2}}{C_{O_2}^{ref}} \right) \left[\exp\left(-\frac{\alpha_c F \eta_c}{RT} \right) - \exp\left(\frac{\alpha_a F \eta_c}{TR} \right) \right] \tag{21}$$

where A_v denotes the electrochemical active area to volume ratio, i_0 denotes the reference exchange current density, C_{ref} denotes the reference concentration of each substance, and α denotes the transfer coefficient.

The driving force behind the chemical reactions in PEMFC is the activation over-potential (η also called activation loss), which can be expressed for the anode and cathode as[30]：

$$\eta_a = (\phi_s - \phi_m) - E_{eq,a} \tag{22}$$

$$\eta_c = (\phi_s - \phi_m) - E_{eq,c} \tag{23}$$

where $E_{eq,a}$ and $E_{eq,c}$ are the equilibrium potentials of the anode and cathode, respectively, whose expressions can be described as[30]：

$$E_{eq,a} = 0 \tag{24}$$

$$E_{eq,c} = E_{Nernst} \tag{25}$$

E_{Nernst} denotes the Nernst equation. In addition, the values of the parameters used for electrochemical transport are listed in Table 3.

Table 3. Electro-chemical transport parameters[27, 30, 31]

Parameters	Unit	Value
Anode transfer coefficient	-	0.5
Cathode transfer coefficient	-	3
Anode reference exchange current density	$A\ m^{-2}$	$1.0e^{-3}$
Cathode reference exchange current density	$A\ m^{-2}$	$1.0e^{2}$
Anode transfer electron number	-	2
Cathode transfer electron number	-	4
Electrical conductivity of electrode	$S\ m^{-1}$	222
Proton conductivity of PEM	$S\ m^{-1}$	9.825
Electrical conductivity of BP	$S\ m^{-1}$	$4.032e^{6}$
H_2_H_2Obinary diffusion coefficient	$m^{2}s^{-1}$	$9.15e^{-5}(T/307.1)^{1.75}$
N_2_H_2Obinary diffusion coefficient	$m^{2}s^{-1}$	$2.56e^{-5}(T/307.15)^{1.75}$
O_2_N_2binary diffusion coefficient	$m^{2}s^{-1}$	$2.2e^{-5}(T/293.2)^{1.75}$
O_2_H_2Obinary diffusion coefficient	$m^{2}s^{-1}$	$2.82e^{-5}(T/308.1)^{1.75}$

2.3 Boundary Conditions

        In setting the boundary conditions of the model, it is assumed that the cell is surrounded by other cells with the same specifications, i.e. the cell model is taken as a duplicate cell in the cell stack. Therefore, the boundaries on both sides of the model are defined as symmetric boundary conditions, and the upper and lower surfaces of the model are periodic boundary conditions. For the external boundary of the cell, it is assumed that the cell undergoes convective heat exchange with the external environment. The operating pressure and operating temperature of the cell are constant. In addition, the potential of the anode plate is set to be zero, the boundary condition is set to be electrical grounding, and the cathode plate is set to be potential. Then, the gas inlet boundary condition of the model takes the velocity inlet and the inlet velocity is calculated based on the stoichiometric ratio, the effective area of the fuel cell (contact area between CH and GDL) and the flow path size as follows[17]:

$$u_{in,a} = \lambda_a \frac{I}{2F} A_{MEA} \frac{1}{x_{H_2}} \frac{RT}{P} \frac{1}{A_{CH}} \qquad (26)$$

$$u_{in,c} = \lambda_c \frac{I}{4F} A_{MEA} \frac{1}{x_{O_2}} \frac{RT}{P} \frac{1}{A_{CH}} \qquad (27)$$

        where $u_{in,a}$ and $u_{in,c}$ are the average inlet velocities of the anode and cathode, respectively. λ_a and λ_c are the stoichiometric numbers of the anode and cathode, respectively. A_{MEA} is the contact area of the channel with the GDL, and A_{CH} is the cross-sectional area of the channel. Both the anode and cathode flow are fully developed flow in the counter-current mode, the anode and cathode outlets use the boundary condition of pressure outlet, and both have zero pressure. The parameter values of the boundary conditions are listed with Table 4.

Table 4. Boundary conditions

| Parameters	Unit	Value
Operation pressure	*Pa*	$101e^3$
Cell temperature	*K*	353.15
Operating voltage	*V*	0.1~0.95
Anode stoichiometry	-	1.2
Cathode stoichiometry	-	2
Anode inlet velocity	*m s^{-1}*	0.372
Cathode inlet velocity	*m s^{-1}*	1.476
Composition of anode inlet gas	-	97%H_2+3%H_2O
Composition of cathode inlet gas	-	77%N_2+20%O_2+3%H_2O
Anode outlet pressure	*pa*	0
Cathode outlet pressure	*Pa*	0

2.4 Model validation
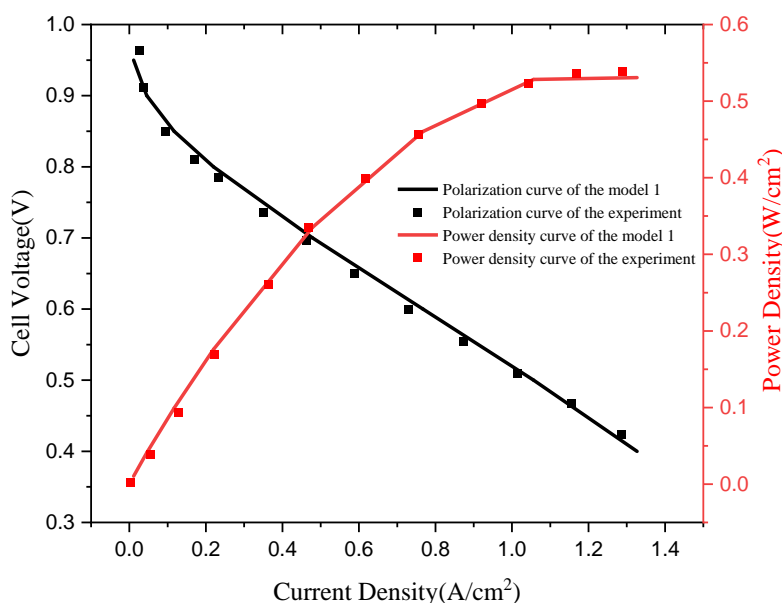
Figure 3. Comparison of simulation results with experimental data

PEMFC involves a variety of physical phenomena, including electrochemical reactions, mass transfer, heat transfer, etc. The complexity of internal reactions also leads to expensive experiments, while numerical studies are not only less expensive, but also yield results that cannot be obtained experimentally, so numerical simulations are widely used in the study of PEMFC. However, numerical studies also need to ensure the correctness of their simulations. The model validation in this study is mainly compared with the experimental data of Ubong[25] and Abdollahzadeh Jamalabadi[26]. (shown in Figure 3.), comparing the current-voltage polarization curve and the power density curve of the cell,

respectively. As can be seen from the figure, both the polarization curve and the power density curve of the cell are in high agreement with the experimental data. Therefore, the validity of the model is proved.

3. RESULTS AND DISCUSSION

In this study, four cell models with rectangular, elliptical, trapezoidal, and dovetail flow channel shapes were developed respectively. The gas flow rate is kept constant by controlling the gas inlet velocity of the cell, the cross-section of the flow channel, and the contact area between the flow channel and the gas diffusion layer to be the same. In contrast to the studies of Huang [21] and Korkischko[22], They only changed the shape of the flow channel and did not control the gas inlet flow rate to keep it constant, the results of which are subject to further debate. The following is a detailed analysis and discussion of the effects of different flow channel shapes on the cell in terms of mass and heat transfer and current density distribution.
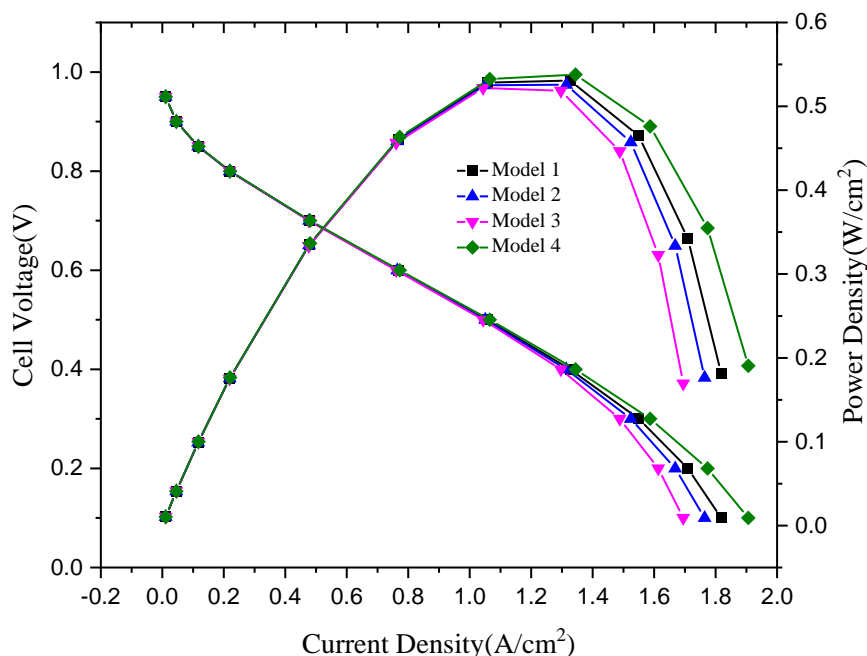
3.1 Cell performance curves

Figure 4. Polarization curves, power density curves of the four models.

Figure 4 shows the polarization curves as well as the power density curves of the four models. It can be seen that among the four models with different flow channels, the flow channel design of Model 4 has a more superior performance. At low current densities, the polarization curves of the four models have less variability. At high current densities, the differences between the polarization curves are more

obvious, and the differences reach the maximum at the corresponding positions of the limiting current density, where the limiting current density of Model 4 is the largest. Such similar results were obtained in Dong's[33] study in analyzing the change of channel shape on the polarization curve and power density curve of the cell (the effect of channel shape on the cell performance is most pronounced at high current density). This indicates that the cross-sectional shape of the channel has a limited effect on the performance of the cell at low current densities. The output power of all four models first increases with increasing current density, and then decreases with increasing current density. The peak output power is achieved around V=0.4 V. The power density peak of Model 4 is the largest, and the power density peak of Model 3 is the smallest. According to the calculation, the peak power density of Model 4 is 6.6% higher than the peak power density of Model 3, and the ultimate current density of Model 4 is 12.5% higher than that of Model 3. Since the channel shape of PEMFC mainly affects the convective and diffusion effects of cell fuel transport. From the analysis of the polarization curve and power density curve, the dovetail flow channel (Model 4) performs better in the mass transfer of the cell, the rectangular flow channel (Model 1) and the elliptical flow channel (Model 2) are in the middle, and the trapezoidal flow channel (Model 3) has the worst mass transfer effect.
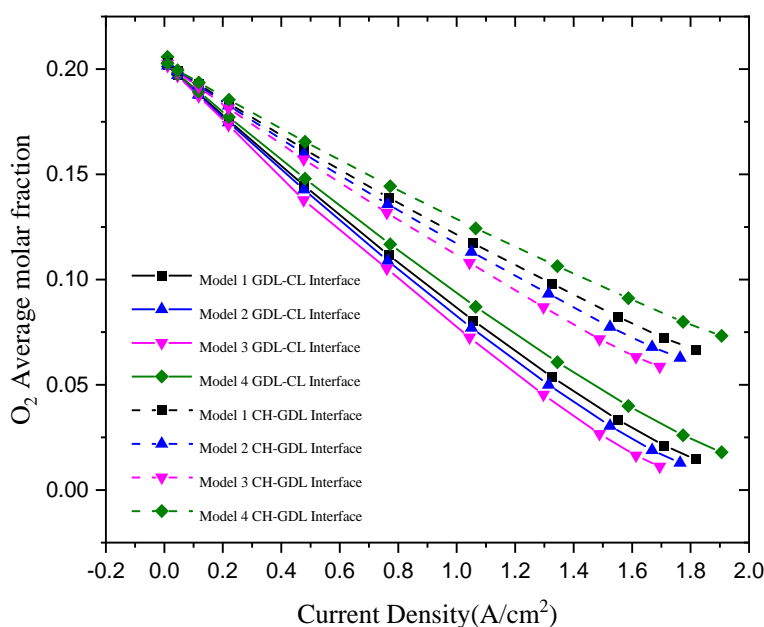
3.2 Oxygen distribution

Figure 5. Average molar fraction of O_2 at different interfaces

The variation of average molar fraction of O_2 at the CH-GDL and GDL-CL interfaces with current density for four different flow channels is shown in Figure 5. It can be seen that the average molar fraction of O_2 decreases with increasing current density, which is mainly due to the fact that the

increased reaction rate results in the need to consume more fuel. In all four models, the average molar fraction of O_2 at the CH-GDL interface is significantly higher than that at the GDL-CL interface. This is because although the GDL is a porous layer through which the gas can pass to the other side, the GDL has a certain thickness and porosity, in which causes a certain resistance of the gas in the diffusion process. In PEMFC, GDL mainly plays the role of fuel buffer and support, but the thickness and porosity of GDL also play a crucial role in the diffusion effect of gas and the elimination of reaction-generated water. In this regard, the material, thickness, porosity and other physical parameters of GDL have been further investigated in order to improve the performance and enhance the hydrothermal management of cell. Besides, at higher current densities, the average O_2 molar fraction of Model 4 is higher than that of other three models at both the CH-GDL and GDL-CL interfaces, and the superiority increases with increasing current density. In terms of material transfer, the dovetail flow channel (Model 4) has the best mass transfer effect.
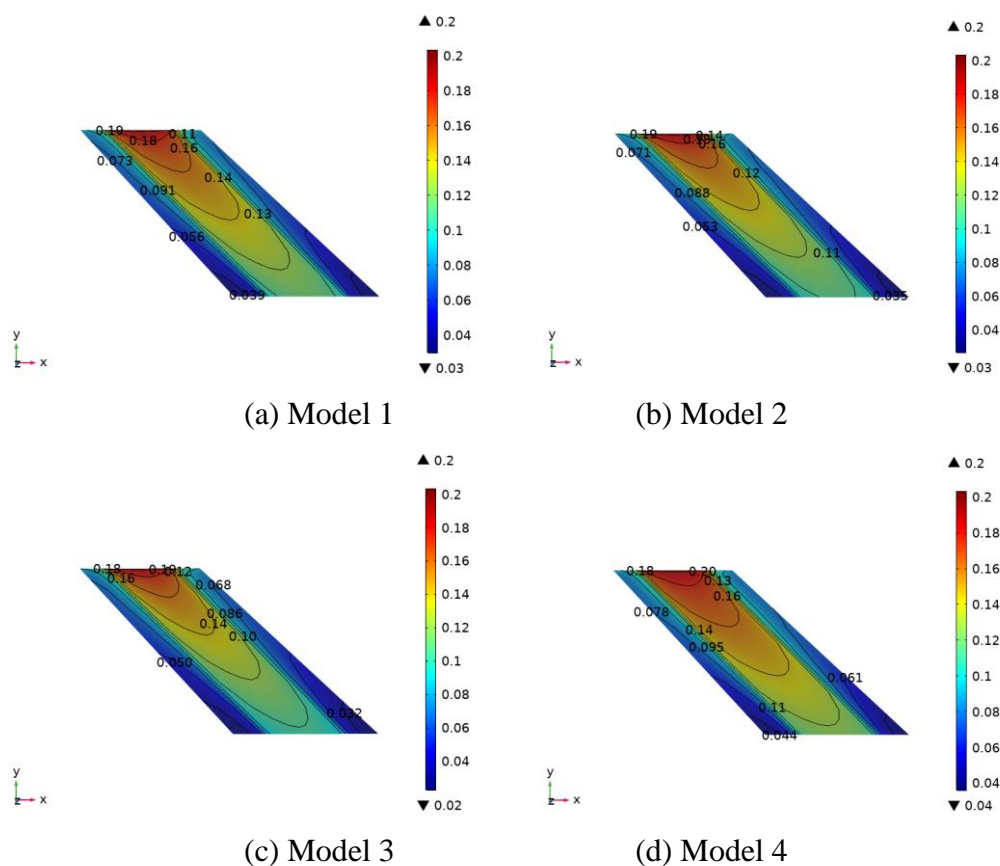

(a) Model 1   (b) Model 2

(c) Model 3   (d) Model 4

Figure 6. Cloud plot of the molar fraction distribution of O_2 at the CH-GDL interface for the four models at *V*=0.4 V

In order to make the distribution of oxygen more uniform, F. Ramin [29] was able to achieve it by widening the channel. Although the uniformity of oxygen distribution at the CH-GDL interface is greatly enhanced to a certain extent, it is also a natural result of expanding the contact area between the

CH and the GDL. In this study, the distribution of oxygen is analyzed by strictly controlling the same contact area between the CH and the GDL. Since the diffusion conditions of the four model GDLs (including the thickness and porosity of the GDLs) are basically the same, the diffusion effects of gases are also basically the same. The shape of flow channel cross-section mainly affects the convection effect of the gas. Figure 6 shows the cloud plot of the molar fraction distribution of O_2 at the CH-GDL interface at 0.4 V for the four cases. As the gas enters the flow channel, the molar fraction of O_2 becomes lower and lower due to the pressure drop of the gas in narrow channel, which leads to an uneven distribution of gas concentration diffusing to the surface of CL. In addition, the O_2 concentration under the runner is significantly higher than under the rib, which is mainly because the gas under the runner is more likely to diffuse to the GDL compared to under the rib. At the inlet, the difference of O_2 molar fraction between the four flow paths is not significant, and the O_2 molar fraction distribution of Model 3 decreases more obviously along the flow path direction as the gas is continuously introduced. At the exit, the O_2 molar fraction of Model 4 is the largest, indicating that the dovetail flow path promotes a more uniform distribution of gas reaching the CL surface. The average molar fractions of O_2 at the CH-GDL interface are 0.09803, 0.09329, 0.0869, and 0.10635 for Models 1~4, respectively.

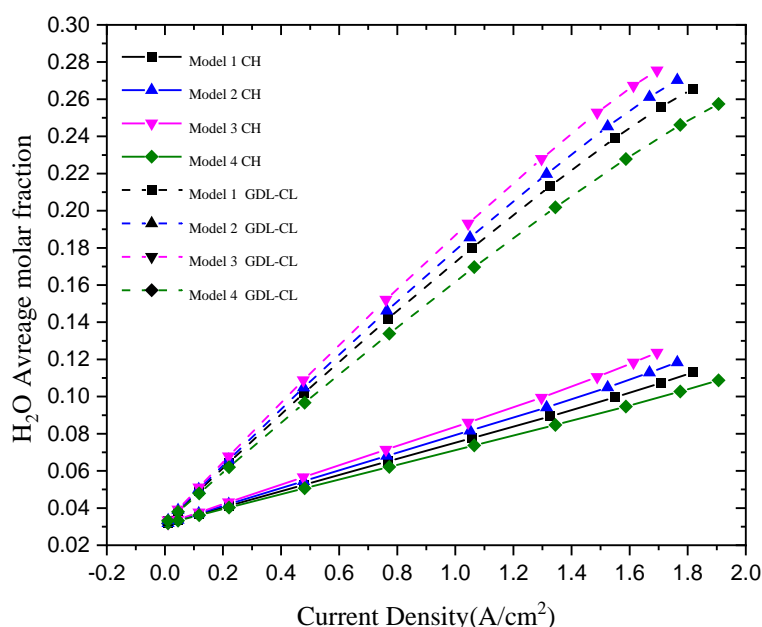### 3.3 Generated water distribution

Figure 7. Average molar fraction of water inside the channel and porous electrode at different current densities.

Water management in PEMFC has always been a hot and important topic. Most of the studies[34-36] have been done by developing new flow paths as a way to efficiently remove the generated water from the cells. In this study, the problem of water content in the cell is analyzed by changing the shape

of the flow channel. Water generation occurs mainly in the cathode chamber, and Figure 7 shows the trend of the average molar fraction of water with current density in the channel and porous electrode (GDL, CL) for the four models. The results showed that with the increase of current density, the water content in both the flow channel and the porous electrode exhibit an increasing trend. This is because oxygen reacts with hydrogen ions and electrons on the surface of the CL of the cathode to generate water, and the higher the current density, the more water is generated, and when the amount of generated water reaches a certain level, the water will break through the GDL and enter the flow channel, which is the main reason why the water content in the flow channel is significantly lower than that in the porous electrode. When excessive water content collects in the channel and GDL, it can impede gas transport. As can be seen in Figure 7, the average water content of Model 3 is the highest in the channel. Similarly, Model 3 has the highest water content among the porous electrodes. This accordingly affects the diffusion effect of oxygen in the Model 3, which in turn affects its performance. In Model 4, where the electrochemical reaction is relatively intense, the water content in the channels and porous electrodes is minimal, mainly due to the fact that Model 4 is able to efficiently drain the generated water through its relatively good convection effect.
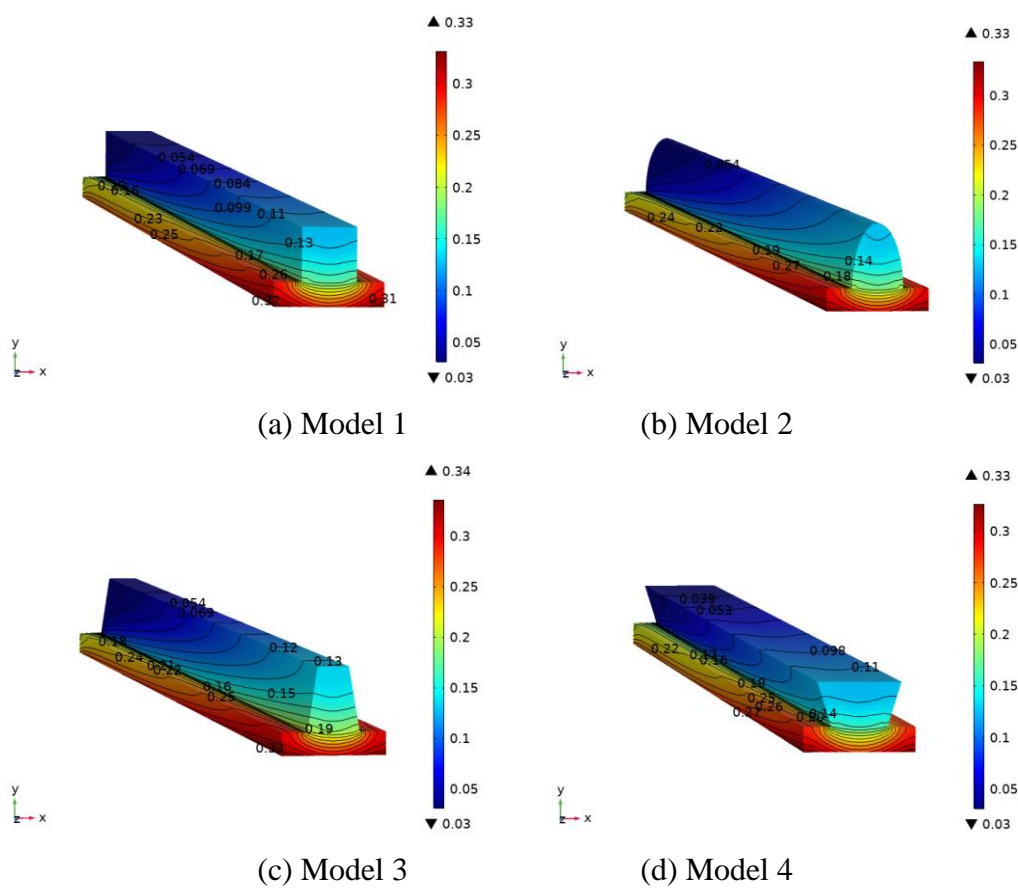

(a) Model 1   (b) Model 2

(c) Model 3   (d) Model 4

Figure 8. Cloud plot of the molar fraction distribution of water generated in the cathode chamber of the four models at *V*=0.4 V.

Figure 8 shows the distribution of water in the cathode chamber for the four models at $V = 0.4$ V. It can be seen that the generated water mainly concentrated in the porous electrode and gradually increases from the inlet to the outlet, which is due to the forward movement of the generated water under the action of the gas flow, and in turn leads to the concentration of water mainly at the outlet of cell. It can be seen from the cloud diagram that the water content under rib is significantly higher than that under channel, which is also mainly due to the gas flow, and the convection effect of the gas facilitating the discharge of the generated water. In the cathode chamber, the average molar fractions of water for Models 1~4 are 0.14807, 0.15378, 0.16027, and 0.140169, respectively. From the contours and the average molar fraction of water in the cathode chamber, Model 1 and Model 4 contribute more to the discharge of generated water compared with Model 2 and Model 3.

3.4 Current density distribution

In PEMFC, hydrogen gas loses electrons in the presence of the anode catalyst, the hydrogen ions which lose electrons reach the surface of the cathode CL through PEM, and the electrons reach the cathode catalytic layer through the external circuit, where oxygen reacts with hydrogen ions and electrons to form water in the presence of catalyst. As electrons are consumed, more electrons reach the cathode side through the external circuit and the directional movement of electrons forms a current. Since the electrochemical reactions in PEMFC mainly occur at the CL-PEM interface, most analytical studies on the current surface density have chosen the CL-PEM interface as the object of study (e.g. ,the study by Xia's study[37]). Figure 9 shows the distribution of the current density at the CL-PEM interface on the cathode side at V=0.4 V, and two important features can be clearly seen: on the one hand, the current density at the CL-PEM interface decreases first and then increases along the direction of oxygen flow, mainly because the fuel inlet of the model is set for counter-current flow, and the hydrogen content is relatively low at the oxygen-rich end, while the oxygen content is relatively low at the hydrogen inlet, thus the current density decreases first and then increases. On the other hand, the current density below the runner is significantly higher than that below the rib. This is due to the fact that the electrochemical reaction occurs mainly in the fuel flow region, and the fuel content below the runners is significantly higher than that below the ribs, thus it appears that the current density below the runners is significantly higher than that below the ribs. It can also be seen from Figure 9 that the maximum values of current density at the CL-PEM interface for all four models are at the oxygen inlet. It is clearly seen that the current density of model 4 has the maximum value. Model 4 has the most uniform current density distribution among the four models with different flow channels. The average current densities (A/m^2) of Model 1~4 at the CL-PEM interface are 11750, 11648, 11506, and 11893, respectively.
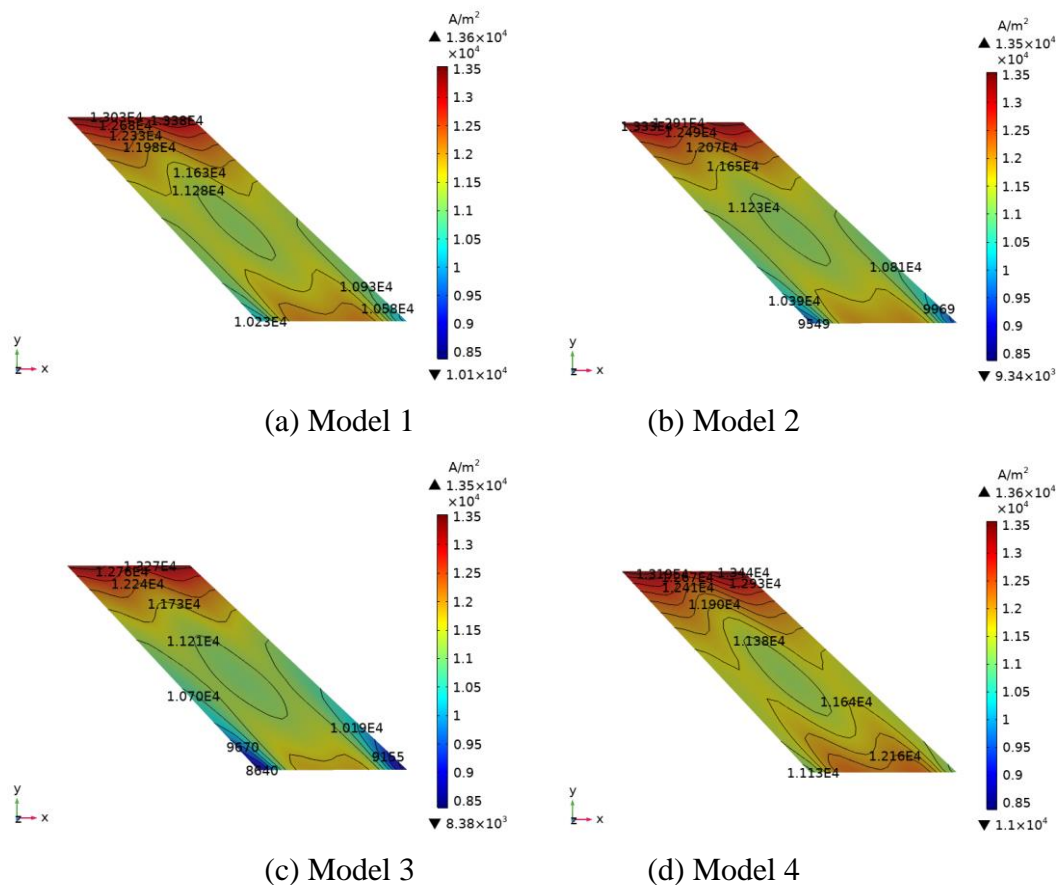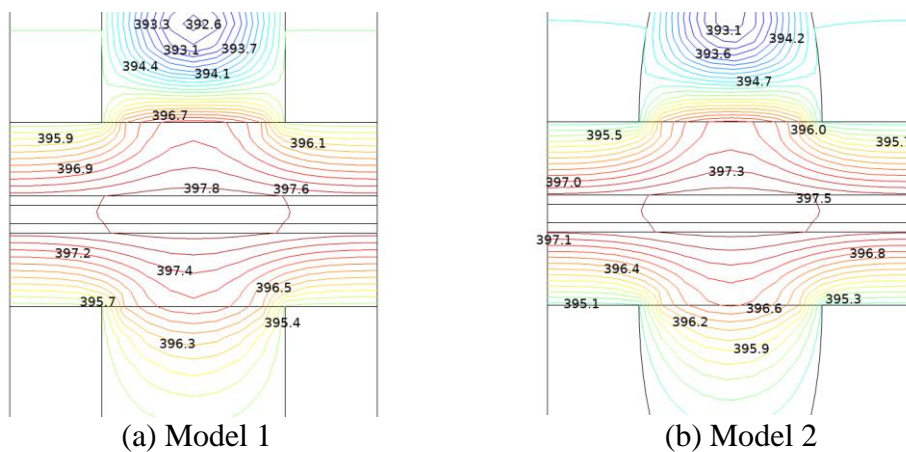
(a) Model 1   (b) Model 2

(c) Model 3   (d) Model 4

Figure 9. Current density distribution at the CL-PEM interface on the cathode side of the four models
       at *V*=0.4 V

3.5 Temperature distribution

(a) Model 1   (b) Model 2
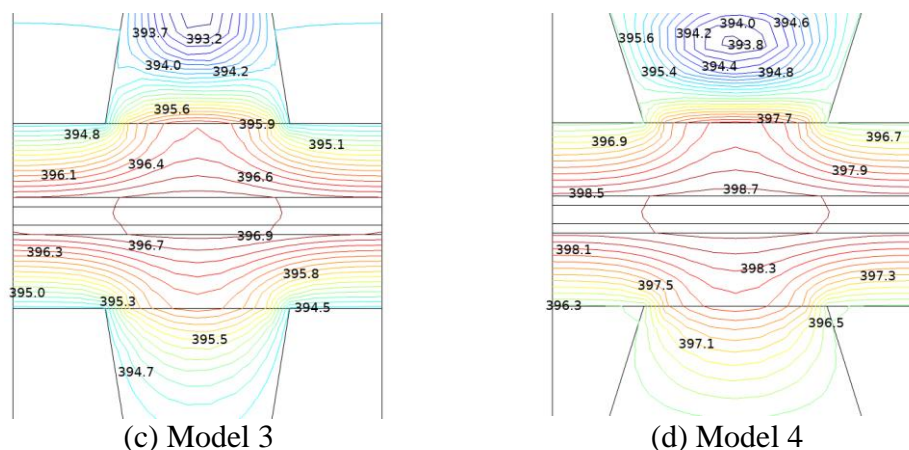
(c) Model 3   (d) Model 4

Figure 10. Temperature (K) distribution of the central section of the four model cells at *V*=0.4v

Thermal management of PEMFC has always been a hot topic. Since the temperature not only affects the activity of the cell catalyst, but also affects the lifetime of the cell. Therefore, it is especially important to investigate the temperature distribution inside the cell. In this study, the center section of the cell is selected as the research object, and its temperature distribution basically tends to be consistent with Oh's research results[38]. Figure 10 shows the temperature distributions of the four models at *V*=0.4 V in the central section of the cell. From the distribution diagram of the temperature contours, it can be seen that the temperature distribution on the cell cross section has the following main characteristics: the temperature of the cathode chamber is higher than that of the anode chamber, and the temperature on the cathode CL is the highest in the cathode chamber. This is mainly due to the fact that the electrochemical reaction of the cell takes place mainly at the cathode CL, where oxygen reacts with protons to produce water and release a large amount of heat at the same time. On the CL, the temperature below the channel is significantly higher than that below the rib in both the cathode and anode chambers. This is due to the relatively slow electrochemical reaction under the rib caused by the low concentration of the reaction gas under the rib, and therefore the relatively low temperature under the rib. In GDL, the closer to the CL the higher its temperature is, which is mainly due to the heat transfer from the porous medium. Meanwhile, the temperature below the rib in GDL is higher than that below the channel. The main reason is that the reaction gas content in the area below the rib is lower, the gas flow is slower and mainly relies on solids for heat transfer, while the gas content in the area below the channel is relatively high and mainly relies on gas flow for heat transport, and the thermal conductivity of solids is much greater than that of gases. Model 3 has the lowest temperature, Model 1 and Model 2 have about the same temperature, and Model 4 has the highest temperature. In summary, the strength of the electrochemical reaction of cell not only determines the magnitude of the resulting current density but also the amount of heat generated.

4. CONCLUSION

BP is an important component in PEMFC, which not only collects current as a connecting carrier of the cell, but also constitutes a channel for gas transport, providing reaction gas to the cell and

excluding produced water. In this study, the fuel cell is numerically simulated by modeling four different shapes of flow channels. And the effect of channel shape on the performance of material transport and current density inside the cell under the direction of gas flow in the cathode chamber is investigated. The main findings are as follows：

1. The influence of flow channel shape on the polarization performance of cell is limited at high operating voltages, which becomes significant as the operating voltage decreases, and the greatest effect occurs when the cell reaches its ultimate current density. The polarization performance of the dovetail shape (Model 4) is optimal, and its ultimate current density is the maximum. Compared to the trapezoidal channel model (Model 3), the dovetail channel model (Model 4) has a 12.5% increase in ultimate current density. This dovetail channel model has the highest peak power density and the trapezoidal channel model has the lowest peak power density.

2. In terms of mass transfer performance, the dovetail shaped channel (Model 4) has a more uniform oxygen distribution compared to the other three channel shapes. The water of the four models is also mainly distributed on the cathode side of the cell, and the water content gradually increases along the gas flow direction. At an operating voltage of 0.4 V, the average water molar fractions of Model 1~4 cathode chambers were 0.14807, 0.15378, 0.16027, and 0.140169, respectively. Among them, model 1 and model 4 show better water removal effect.

3. For the current density distribution, the average current densities (A/m^2) at the CL-PEM interface for Model 1~4 at an operating voltage of 0.4 V are 11750, 11648, 11506, and 11893, respectively. The average current density of the Model 4 is 387 (A/m^2) higher than that of the Model 3, mainly due to the difference in gas fuel delivery mentioned above.

4. For the temperature distribution of the fuel cell, the model center section is selected as the object of study in this paper. It has been shown that the temperature of the fuel cell reaches a maximum at the CL on the cathode side. Among the four models, the temperature of Model 4 is the highest. This is because the electrochemical reaction occurs mainly on the CL of the cell, and the higher the intensity of the electrochemical reaction the more heat is generated.

CONFLICT OF INTEREST
The authors declared that there is no conflict of interest.

DATA AVAILABILITY
The data that support the findings of this study are available from the corresponding author upon reasonable request.

References

1.   A. Kalathil, A. Raghavan and B. Kandasubramanian, *Polymer-Plastics Technology and*

Materials, 58(2018) 465.

2.   J. C. Kurnia, A. P. Sasmito and T. Shamim, *Applied Energy,* 252(2019) 113416.
3.   X. Lü, Y. Qu, Y. Wang, C. Qin and G. Liu, *Energy Conversion and Management,* 171(2018) 1273.
4.   M. Arif, S. C. P. Cheung and J. Andrews, *Energy & Fuels,* 34(2020) 11897.
5.   R. F. Silva, D. Franchi, A. Leone, L. Pilloni, A. Masci and A. Pozio, *Electrochimica Acta,* 51(2006) 3592.
6.   C. W. Wu, W. Zhang, X. Han, Y. X. Zhang and G. J. Ma, *Journal of Power Sources,* 476(2020) 228724.
7.   S. Wu, W. Yang, H. Yan, X. Zuo, Z. Cao, H. Li, M. Shi and H. Chen, *International Journal of Hydrogen Energy,* 46(2021) 8672.
8.   T. Wilberforce, Z. El-Hassan, F. N. Khatib, A. Al Makky, A. Baroutaji, J. G. Carton, J. Thompson and A. G. Olabi, *International Journal of Hydrogen Energy,* 42(2017) 25639.
9.   H.-K. Ma, S.-H. Huang, J.-S. Wang, C.-G. Hou, C.-C. Yu and B.-R. Chen, *Journal of Power Sources,* 195(2010) 1393.
10.   C. Min, J. He, K. Wang, L. Xie and X. Yang, *Energy Conversion and Management,* 180(2019) 1217.
11.   J. Shi, H. Xu, H. Zhao, L. Lu and X. Wu, *Journal of Power Sources,* 252(2014) 189.
12.   T. Chen, S. Liu, S. Gong and C. Wu, *International Journal of Energy Research,* 37(2013) 1680.
13.   A. A. Ebrahimzadeh, I. Khazaee and A. Fasihfar, *Heliyon,* 4(2018) e00974.
14.   D. Jeon, *International Journal of Hydrogen Energy,* 33(2008) 1052.
15.   S.-W. Perng and H.-W. Wu, *Applied Energy,* 143(2015) 81.
16.   X. Wang, Y. Qin, S. Wu, X. Shangguan, J. Zhang and Y. Yin, *Journal of Power Sources,* 457(2020) 228034.
17.   X.-W. Zhang, X.-J. Wang, X.-Z. Cheng, L. Jin, J.-W. Zhu and T.-T. Zhou, *Energy,* 207(2020) 118141.
18.   A. P. Manso, F. F. Marzo, J. Barranco, X. Garikano and M. Garmendia Mujika, *International Journal of Hydrogen Energy,* 37(2012) 15256.
19.   Z. Wan, W. Quan, C. Yang, H. Yan, X. Chen, T. Huang, X. Wang and S. Chan, *Energy Conversion and Management,* 205(2020) 112386.
20.   D. H. Ahmed and H. J. Sung, *Journal of Power Sources,* 162(2006) 327.
21.   T. Huang, W. Wang, Y. Yuan, J. Huang, X. Chen, J. Zhang, X. Kong, Y. Zhang and Z. Wan, *Energy Reports,* 7(2021) 1374.
22.   I. Korkischko, B. S. Carmo and F. C. Fonseca, *Fuel Cells,* 17(2017) 809.
23.   L. S. Freire, E. Antolini, M. Linardi, E. I. Santiago and R. R. Passos, *International Journal of Hydrogen Energy,* 39(2014) 12052.
24.   C. Li, X. Xu, H. Hu, N. Mei and Y. Yang, *International Journal of Energy Research,* 45(2020) 7719.
25.   E. U. Ubong, Z. Shi and X. Wang, *J Electrochem Soc,* 156(2009) B1276.
26.   M. Yaghoub Abdollahzadeh Jamalabadi, M. Ghasemi, R. Alamian, E. Afshari, S. Wongwises, M. Mehdi Rashidi and M. Safdari Shadloo, *Applied Sciences,* 9(2019) 3633.
27.   S.-y. Zhang, Z.-g. Qu, H.-t. Xu, F.-K. Talkhoncheh, S. Liu and Q. Gao, *International Journal of Hydrogen Energy,* 46(2021) 27700.
28.   J. Son, D. Lee, S. Um and Y.-B. Kim, *Energy Conversion and Management,* 232(2021) 113803.
29.   F. Ramin, H. Sadeghifar and A. Torkavannejad, *International Journal of Heat and Mass Transfer,* 129(2019) 1151.
30.   L. Xia, M. Ni, Q. He, Q. Xu and C. Cheng, *Applied Energy,* 300(2021) 117357.
31.   M. Liu, H. Huang, X. Li, X. Guo, T. Wang and H. Lei, *International Journal of Hydrogen Energy,* 46(2021) 37379.
32.   Y. Cai, D. Wu, J. Sun and B. Chen, *Energy,* 222(2021) 119951.

Int. J. Electrochem. Sci., 17 **(2022)** Article Number: 220319

20

33.   P. Dong, G. Xie and M. Ni, *Energy,* 206(2020) 117977.
34.   K. Jiao and X. Li, *Progress in Energy and Combustion Science,* 37(2011) 221.
35.   B. H. Lim, E. H. Majlan, W. R. W. Daud, T. Husaini and M. I. Rosli, *Ionics,* 22(2016) 301.
36.   H. Liu, *International Journal of Electrochemical Science,* 15(2020) 6717.
37.   L. Xia, Q. Xu, Q. He, M. Ni and M. Seng, *International Journal of Hydrogen Energy,* 46(2021) 21098.
38.   K. Oh, P. Chippar and H. Ju, *International Journal of Hydrogen Energy,* 39(2014) 2785.